crystals

MDPI

Article

Effects of Synthesis Parameters on Crystallization Behavior of K-MER Zeolite and Its Morphological Properties on Catalytic Cyanoethylation Reaction

Ying-Wai Cheong [1], Ka-Lun Wong [2], Boon Seng Ooi [3], Tau Chuan Ling [4], Fitri Khoerunnisa [5] and Eng-Poh Ng [1,*]

1 School of Chemical Sciences, Universiti Sains Malaysia, Penang 11800 USM, Malaysia; thia911@hotmail.com
2 School of Energy and Chemical Engineering, Xiamen University Malaysia, Jalan Sunsuria, Bandar Sunsuria, Sepang 43900, Selangor, Malaysia; kalun.wong@xmu.edu.my
3 School of Chemical Engineering, Engineering Campus, Universiti Sains Malaysia, Seri Ampangan, Nibong Tebal 14300, Penang, Malaysia; chobs@usm.my
4 Institute of Biological Sciences, Faculty of Science, University of Malaya, Kuala Lumpur 50603, Malaysia; tcling@um.edu.my
5 Chemistry Education Department, Universitas Pendidikan Indonesia, Jl. Setiabudhi 258, Bandung 40514, Indonesia; fitri.khoerunnisa@gmail.com
* Correspondence: epng@usm.my

Received: 24 December 2019; Accepted: 19 January 2020; Published: 23 January 2020

Abstract: MER-type zeolite is an interesting microporous material that has been widely used in catalysis and separation. By carefully controlling the synthesis parameters, a procedure to synthesize K-MER zeolite crystals with various morphologies has been developed. The silica, water and mineralizer content in the synthesis gel, as well as crystallization time and temperature, have a profound impact on the crystallization kinetics, resulting in zeolite solids with various degrees of crystallinity, crystal sizes and shapes. K-MER zeolite crystals with nanorod, bullet-like, prismatic and wheatsheaf-like morphologies have been successfully obtained. The catalytic performances of the K-MER zeolites in cyanoethylation of methanol, under novel non-microwave instant heating, have been investigated. The zeolite in nanosize form shows the best catalytic performance (94.1% conversion, 100% selectivity) while the bullet-like zeolite gives poorest catalytic performance (44.2% conversion, 100% selectivity).

Keywords: K-MER zeolite; synthesis parameter; morphology; cyanoethylation of methanol; catalyst

1. Introduction

Zeolites are crystalline microporous aluminosilicates formed by a network of $[SiO_4]^{4-}$ and $[AlO_4]^{5-}$ tetrahedrals [1]. These materials have unique properties, such as their uniform microporous structure, hydrophilic surfaces, adjustable framework composition and strong chemical interactions with guest molecules. These properties have made them suitable candidates for widespread applications, including gas separation, adsorption, ion-exchange and catalysis [2–8]. The search for new materials is important especially for the petrochemical and pharmaceutical industries. In particular, potassium containing MER zeolite (K-MER), a zeolite which has framework topology similar to the mineral merlinoite; has drawn researchers' attention due to its three-dimensional pore channel system with medium pore sizes and high hydrophilicity. Thus, it is a promising material for adsorption [9], separation [10], and catalytic applications [11,12].

The physicochemical properties of zeolites are greatly dependent on their framework structures. Furthermore, the morphological properties such as crystal shape and size of a zeolite also have

great impact on their physicochemical properties and applications [13,14]. For example, the shape of zeolite crystals has been shown to exert a significant effect in adsorption and separation applications since it modulates molecular diffusion, accessibility, interfacial energy, molecular separation and inclusion properties [15,16]. Recently, several techniques to control the morphological properties of zeolites were reported [17]. For example, the use of different organic templates has shown to produce AlPO-5 zeolite-like materials with aggregated sphere, plate, rod, prism and barrel shapes [18–20]. The employment of different heating methods such as microwave and ultrasonic radiations exhibit significant effects on the overall crystal size and shape of the zeolite products [21,22]. In addition, the influence of the hydrothermal synthesis parameters, such as silica and alumina contents, alkalinity, amount of water, type of organic template, type of mineralizer, crystallization time and temperature, on the morphological and other properties of zeolites are also reported [23–25]. Nevertheless, knowledge about the impact of these synthesis parameters on the morphological behavior, crystallization kinetics and formation process of K-MER zeolite is still not well understood.

Therefore, we have studied the influence of synthesis parameters on the formation of K-MER zeolite (e.g. crystallization kinetics, structure and purity, morphology and crystal size). In addition, the influence of crystal morphologies on the catalytic behavior of K-MER zeolite in the cyanoethylation of methanol, under novel non-microwave instant heating, is also presented in this paper.

2. Experimental

2.1. Synthesis of MER Zeolite

The synthesis of MER zeolite (W-3) was carried out as follows. Typically, $Al(OH)_3$ (1.448 g, extra pure, Acros Organics) and KOH (4.290 g, 85%, QRëC) were mixed in distilled water (11.876 g). The mixture was magnetically stirred at 100 °C for 16 h. The clear aluminate solution was then slowly introduced into the silicate solution comprising HS-40 (9.763 g, 40% SiO_2, Sigma–Aldrich) and distilled water (15.022 g). The resulting hydrogel with a molar composition of $1Al_2O_3$:$7SiO_2$:$3.5K_2O$:$196H_2O$ was stirred for another 10 min before crystallization at 180 °C for 14 h. The solid product obtained was purified with distilled water using high speed centrifugation (10,000 rpm, 10 min) until pH 7 and the sample was freeze-dried. Other samples were also prepared by varying the synthesis conditions as summarized in Table 1 using the same procedure. The samples were labelled as W-*n* where *n* was the number of the sample.

2.2. Characterization

The XRD patterns of the samples were recorded using a Bruker AXS D8 (MA, USA) diffractometer with Cu-Kα radiation (λ = 1.5418 Å) at 2θ = 3–50°. The morphology of solids was studied with a FESEM microscope (Leo Supra 50VP, Oberkochen, Germany) operating at 20 kV. The average crystal size of solids was determined using ImageJ software by counting 50 crystals randomly throughout the FESEM images. The Si/Al and K/Al ratios of the solids were determined by using a Perkin Elmer's atomic absorption spectrometer (AAS, AAnalyst 400). Prior to analysis, the sample was dissolved in hydrofluoric acid solution (0.5 M) where boric acid was also added to minimize the fluoride interference. Meanwhile, five standard solutions of each Al, Si and K elements were also prepared for calibration study. The surface area of the samples was calculated by using the BET equation where the monolayer volume (V_{mono}) was first obtained from the nitrogen adsorption isotherm; the samples were first degassed (6 h, 300 °C) before the adsorption isotherms were recorded from a Micrometrics ASAP 2010 analyzer (Norcross, USA) at −196 °C. The surface basicity of MER zeolite samples was analyzed using a BELCAT-B temperature programmed desorption (TPD) instrument (Osaka, Japan). Initially, the solid sample (ca. 100 mg) was outgassed at 450 °C overnight before CO_2 gas was introduced for adsorption. The excess CO_2 was then evacuated at room temperature and CO_2 desorption was performed from 40 to 500 °C at a heating rate of 10 °C /min. The TPD profile was plotted as TCD signal versus desorption temperature.

2.3. Catalytic Study

Catalytic cyanoethylation of methanol was performed using the following procedure. First, K-MER zeolite (0.500 g), methanol (28 mmol, Merck) and acrylonitrile (7 mmol, Merck) were loaded into a 10-mL quartz vial. The vial was sealed with a silicon cap, heated (140 °C) and magnetically stirred (800 rpm) in a non-microwave instant heating reactor (Anton Paar's Monowave 50, Graz, Austria) for several specific heating times (0-90 min). After cooling down, the reaction solution was isolated from the solid catalyst and injected into a GC–MS (Perkin-Elmer Clarus 500 system, Massachusetts, USA) and a GC–FID (Agilent/HP 6890 GC, Califonia, USA) for identification and quantitative analysis, respectively.

3. Results and Discussion

3.1. Effect of Heating Time

The crystallization of K-MER zeolite was first studied by varying the hydrothermal heating times at 180 °C. An amorphous solid product was formed at 0 h according to the XRD analysis where a strong broad XRD hump at 2θ = 22.3° was detected (Figure 1a: W-1). The XRD data was supported by FESEM observation of nanoparticles (ca. 58 nm) with coral-like structure (Figure 2a). With a heating time of 10 h, a significant drop in the Si/Al ratio from 7.81 to 3.73 was observed in the solids (Table 1). Yet, no crystalline phase was revealed by XRD technique at this time. Nevertheless, the amorphous hump became weaker and shifted to 2θ = 27.8° (Figure 1b: W-2). Both XRD and AAS elemental analyses thus revealed the occurrence of amorphous phase reorganization into secondary more reactive amorphous solid at 10 h [26]. This amorphous-amorphous phase transformation was also confirmed by FESEM study where bulkier amorphous entities (ca. 180 nm) were formed (Figure 2b). Interestingly, the appearance of particles with more well-defined nanorod morphology (ca. 33 × 4 nm^2) was detected randomly in W-2 sample via microscopic investigation. This indicated that the nucleation process of K-MER zeolite had occurred. These nanorods were agglomerated into bundle-like secondary particles (ca. 650 nm) and were grown on the surface of an amorphous particle.

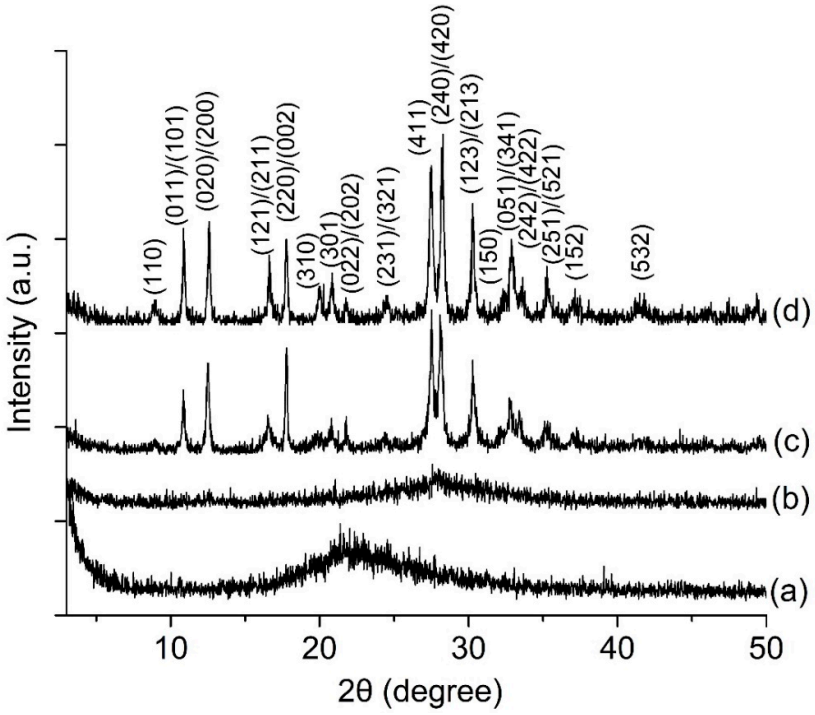

Figure 1. XRD patterns of (**a**) W-1, (**b**) W-2, (**c**) W-3 and (**d**) W-4 samples heated for 0, 10, 14 and 20 h, respectively.

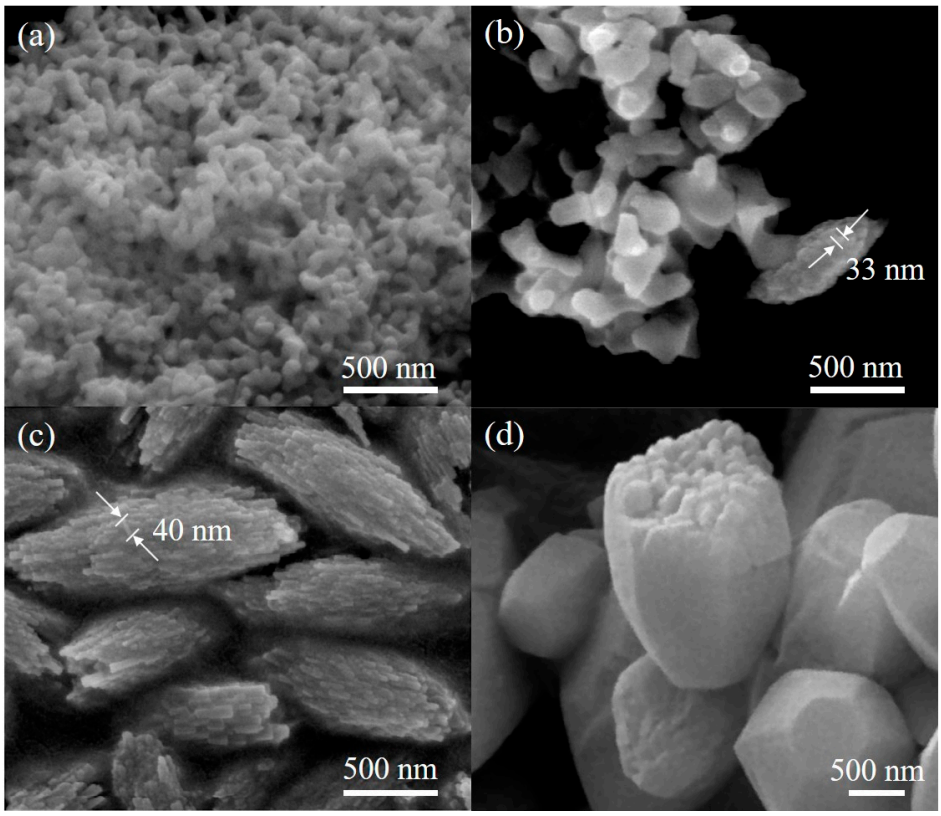

Figure 2. FESEM images of (**a**) W-1, (**b**) W-2, (**c**) W-3 and (**d**) W-4 samples heated for 0, 10, 14 and 20 h, respectively.

Table 1. The chemical compositions of precursor hydrogels and their respective synthesis conditions.

Parameters	Samples	Gel Molar Composition				T (°C)	t (h)	Si/Al Ratio	Phase(s) [a]
		SiO_2	Al_2O_3	K_2O	H_2O				
Time	W-1	7	1	3.5	196	180	0	7.81	Am.
	W-2						10	3.73	Am.>>MER
	W-3						14	2.29	MER
	W-4						20	2.28	MER
Temperature	W-5	7	1	3.5	196	120	14	3.29	Am.
	W-6					140		2.63	MER
	W-7					160		2.61	MER
	W-3					180		2.29	MER
K_2O	W-3	7	1	3.5	196	180	14	2.29	MER
	W-8			5.0				2.29	MER
	W-9			7.0				2.28	MER
SiO_2	W-10	1.5	1	3.5	130	180	14	1.22	EDI
	W-11	5						2.53	MER
	W-12	7						2.73	LTL<MER
	W-13	10						3.05	LTL
H_2O	W-14	7	1	3.5	100	180	14	2.82	LTL<MER
	W-12				130			2.73	LTL<MER
	W-3				196			2.29	MER
	W-16				280			2.31	MER

[a] Am. = Amorphous.

When the heating time was prolonged to 14 h, the amorphous solids were completely consumed as nutrient and subsequently crystalline K-MER zeolite nanocrystals were produced (Figure 1c: W-3). At this time, the Si/Al ratio became nearly constant, with a value of 2.29. As shown in Figure 2c,

the crystalline primary (ca. 40 nm) and secondary (ca. 1.3 μm) particles had grown to a larger size due to simultaneous occurrence of nucleation and crystal growth processes. The XRD analysis also supported this conclusion, as no amorphous hump was seen in the XRD pattern (Figure 1c). Indeed, the pattern showed major peaks at 2θ = 8.96°, 10.84°, 12.46°, 16.58°, 17.80°, 27.50°, 28.10°, 30.28° and 32.88° which were characteristics of the MER framework topology [27]. Further increasing the heating time to 20 h showed no change in the framework composition and framework type but the XRD peaks with higher intensity and narrower peaks were recorded (Figure 1d: W-4), indicating Ostwald ripening and crystal growth were dominating the crystallization process [28]. This was supported by the FESEM microscopy showing that the crystalline K-MER zeolite nanorods further agglomerated and transformed into larger MER crystals (>1 μm) with bullet-shape morphology.

3.2. *Effect of Heating Temperature*

Heating temperature plays a very crucial role in zeolite crystallization process as it provides energy to overcome the activation energy of the reactions (polycondensation, induction, nucleation, crystal growth, etc.) [29,30]. Hence, the hydrogel with the same molar composition ($1Al_2O:7SiO_2:3.5K_2O:196H_2O$) was subjected to hydrothermal treatment at 120, 140, 160 and 180 °C for 14 h. The W-5 solid product appeared to be amorphous at 120 °C and the Si/Al ratio of the solid was 3.29 (Figures 3a and 4a, Table 1). The chemical composition reached nearly 2.60 when the synthesis temperature was raised to 140 °C. At this temperature, K-MER zeolite nanorods (ca. 28 nm) were obtained which tend to form secondary agglomerated particles of ca. 240 nm (Figures 3b and 4b: W-6). Upon increasing the temperature to 160 °C (W-7) and 180 °C (W-3), no change in the framework chemical composition (Si/Al ratio) and crystalline phase were detected but the size of primary and secondary particles became larger due to further crystals growth at higher temperature (Figure 3c,d and Figure 4c,d). The results indicate that the crystallization of MER zeolite is a thermally activated reaction.

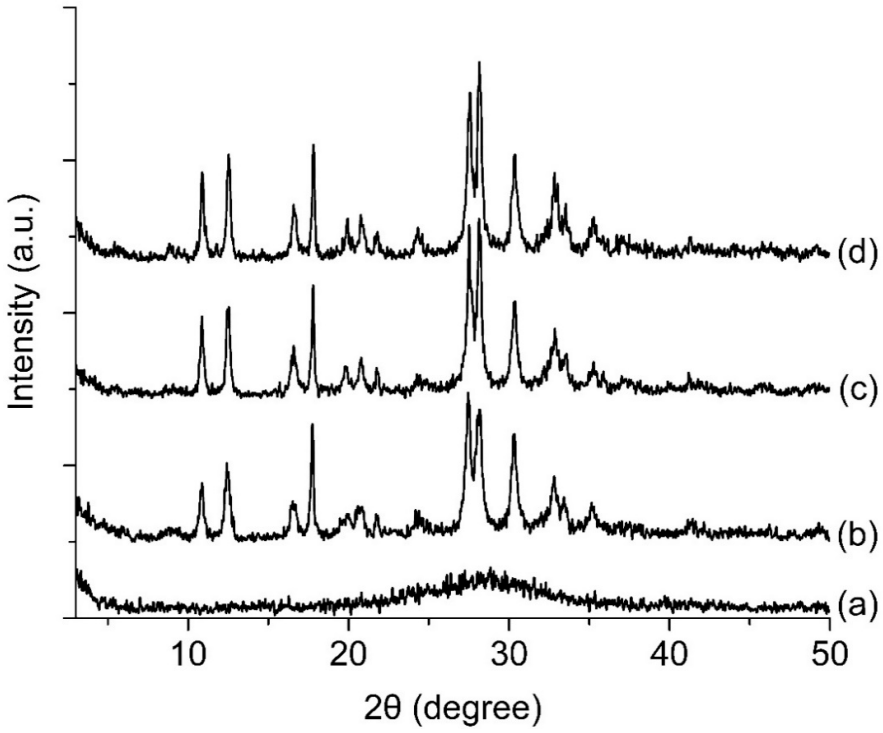

Figure 3. XRD patterns of (**a**) W-5, (**b**) W-6, (**c**) W-7 and (**d**) W-3 samples upon heating at 120, 140, 160 and 180 °C for 14 h, respectively.

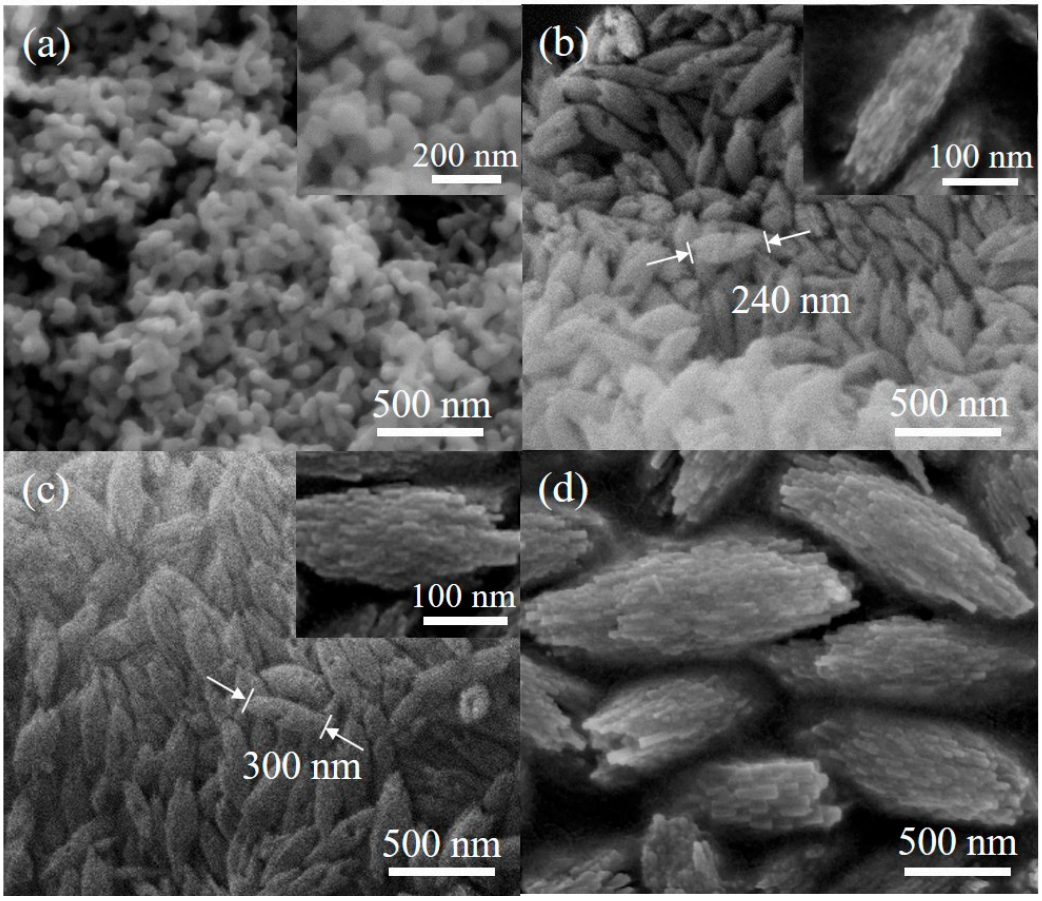

Figure 4. FESEM images of (**a**) W-5, (**b**) W-6, (**c**) W-7 and (**d**) W-3 samples upon heating at 120, 140, 160 and 180 °C for 14 h, respectively.

3.3. Effect of K_2O Content

Mineralizer is an essential chemical component in the synthesis of zeolites as it increases the overall solubility of inorganic species in the precursor hydrogels by providing accessibility to useful species at a level needed for the nucleation and crystal growth of zeolites. Hence, a precursor hydrogel with a composition of $7SiO_2$: $1Al_2O_3$: xK_2O: $196H_2O$ (x = 3.5, 5.0 and 7.0) was heated at 180 °C for 14 h to study the effect of K_2O mineralizer. From the XRD data, the framework chemical composition and the purity of crystallized products remained intact with no other competing phases detected in the K_2O range studied (Table 1, Figure 5). However, a change in the crystal morphology was observed upon varying the K_2O content. At x = 3.5 (W-3), the obtained crystals were in nanorod morphology, while a mixing of nanorods and prismatic crystals were observed at x = 5.0 (W-8), demonstrating the significant effect of mineralizer content on the morphological properties of K-MER zeolite (Figure 6a). A similar observation was also reported by Zhang et al. where the addition of a higher amount of NaOH as mineralizer promotes the crystal growth at a specific axis, resulting in the crystallization of silicalite-1 zeolite with spherical shape instead of common coffin shape [31]. Further increasing the K_2O content (x = 7.0: W-9) led to the formation of K-MER zeolite with only pure prismatic-shape crystals (Figure 6c). As seen, the average size of prismatic shape crystals also reduced from 125 × 167 nm^2 to 114 × 160 nm^2 when the K_2O content increased due to the enhancement of the solubility of aluminosilicate species as a result of higher alkalinity in the hydrogel solution [32].

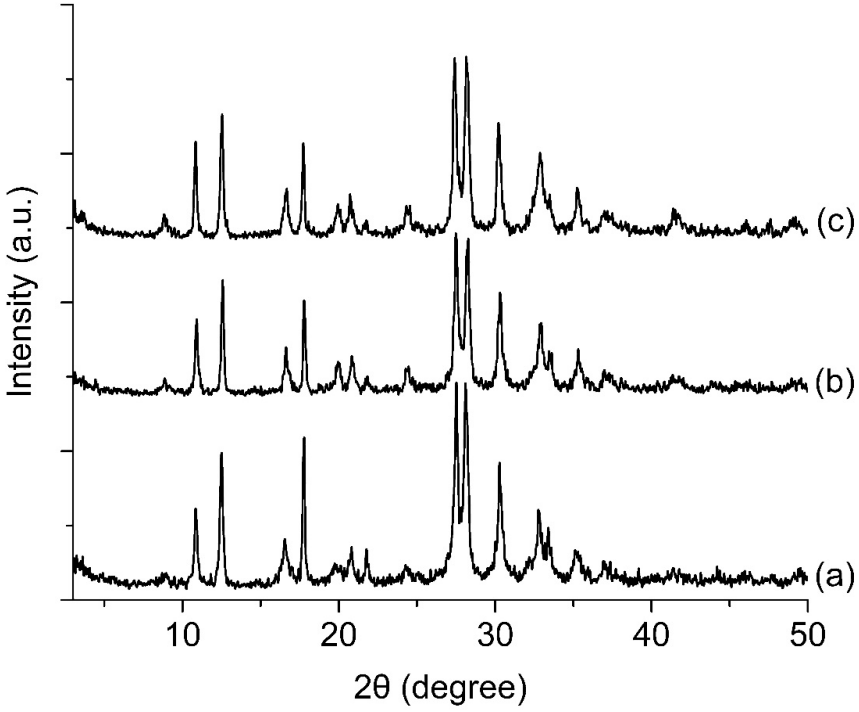

Figure 5. XRD patterns of samples prepared from an aluminosilicate gel precursor with a composition of $7SiO_2$: $1Al_2O_3$: xK_2O: $196H_2O$ with x = (**a**) 3.5 (W-3), (**b**) 5 (W-8) and (**c**) 7 (W-9). All samples were heated at 180 °C for 14 h.

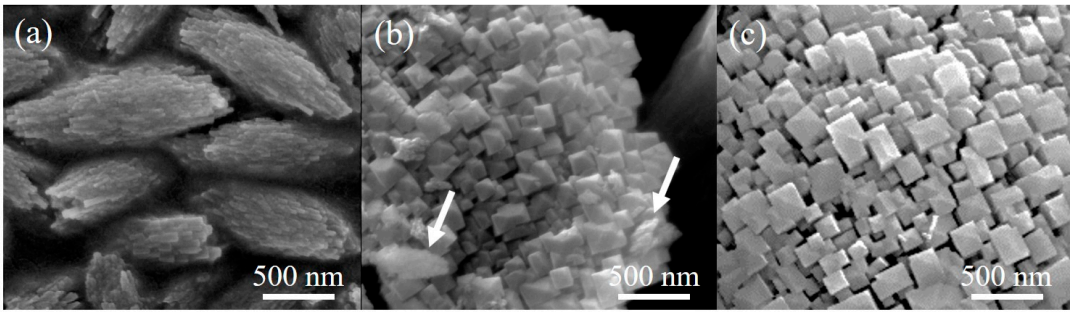

Figure 6. FESEM images of (**a**) W-3, (**b**) W-8 and (**c**) W-9 samples prepared from an aluminosilicate gel precursor with the composition of $7SiO_2$: $1Al_2O_3$: xK_2O: $196H_2O$ with x = 3.5, 5 and 7, respectively. The arrows shown in (**b**) indicate the existence of K-W nanorod crystals in midst of K-W prismatic crystals.

3.4. Effect of SiO_2 Content

The effect of SiO_2 content was also studied ranging from SiO_2/Al_2O_3 = 1.5 to 10. The results showed that the phase purity was found to be more sensitive by varying the SiO_2 content as compared to the K_2O content and heating temperature (Table 1). Crystalline W-10 with a high silica content (Si/Al ratio = 1.22) and cubic morphology was obtained when the hydrogel with low silica content (SiO_2/Al_2O_3 ratio = 1.5) was used. The solid was proven to be an EDI-type zeolite according to XRD and SEM analyses (Figures 7a and 8a). At a SiO_2/Al_2O_3 molar ratio of 5.0, W-11 (Si/Al ratio = 2.53) with a pure MER crystalline phase was produced (Figures 7b and 8b). Further increasing the silica content led to the co-crystallization of MER- and LTL-type zeolites before single phase of LTL-type zeolite product was crystallized at a SiO_2/Al_2O_3 molar ratio of 10 (Figure 7c,d and Figure 8c,d). As shown, the LTL-type zeolite (W-13), having a one-dimensional pore structure, possessed a higher framework silica content (Si/Al ratio = 3.05) and exhibited a novel spinning top-like shape instead of conventional cylindrical structure [33] owing to the silica source and the precursor molar composition used.

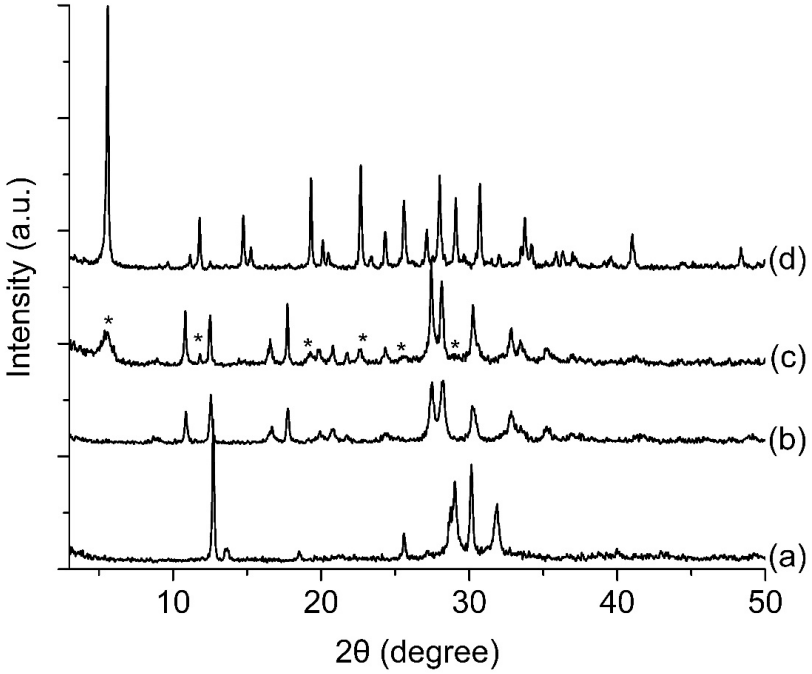

Figure 7. XRD patterns of (**a**) W-10, (**b**) W-11, (**c**) W-12 and (**d**) W-13 samples crystallized at 180 °C for 14 h using an aluminosilicate gel precursor of $y$$SiO_2$:1$Al_2O_3$:3.5$K_2O$:130$H_2O$ where y = 1.5, 5, 7 and 10, respectively. The * marks in (**c**) indicate the presence of the LTL crystalline phase.

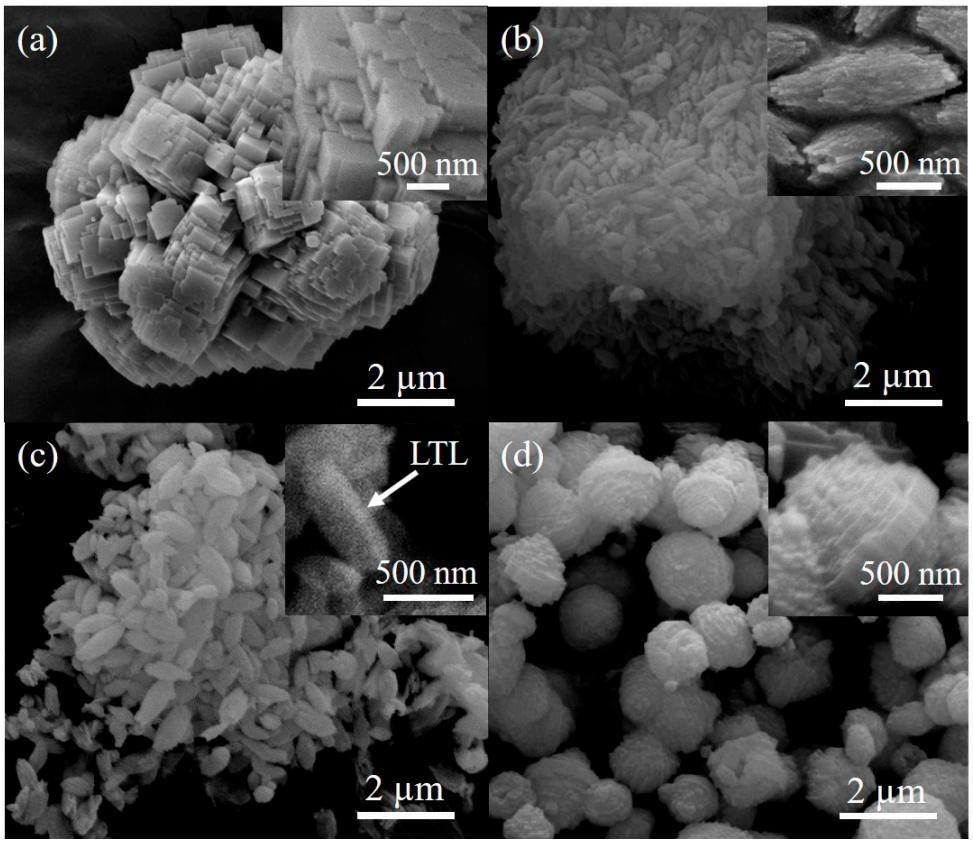

Figure 8. FESEM images of solids prepared using a precursor hydrogel of $y$$SiO_2$:1$Al_2O_3$:3.5$K_2O$: 130$H_2O$ at 180 °C for 14 h where y = (**a**) 1.5 (W-10), (**b**) 5 (W-11), (**c**) 7 (W-12) and (**d**) 10 (W-13).

3.5. Effect of Water Content

Water content plays an important role in the hydrothermal synthesis of zeolites. It not only serves as a solvent during the crystallization process, but also regulates the formation of possible precursors of zeolite frameworks [34]. Hence, the crystallization of K-MER zeolite was studied at 180 °C for 14 h by varying the molar ratio of water from 100 to 280 (Table 1). At low water content (H_2O/Al_2O_3 = 100: W-14), LTL crystalline phase was co-crystallized with the MER crystalline phase (Figure 9a). This observation could also be confirmed by the AAS spectroscopy results where the Si/Al ratio of solid was 2.82 indicating the mixing of both high silica (LTL) and low silica (MER) zeolites. The results were further supported by FESEM analysis where cylindrical nanorods of ca. 350 × 970 nm^2, which were characteristic of LTL-type zeolite, were observed and grown together with the K-MER nanocrystals (Figure 10a). The LTL crystalline phase, however, slowly disappeared with increasing water content, indicating the direct influence of water on the crystallization of LTL-type zeolite. At higher H_2O/Al_2O_3 ratios (196–280), zeolites of pure MER crystalline phase with different crystallite sizes and morphologies were obtained. As shown, the bundle-like MER-type zeolite particles made up of nanorod primary crystals (205 × 40 nm^2) were captured at H_2O/Al_2O_3 = 196 (Figures 9c and 10c: W-3). The nanocrystals grew further, and larger secondary crystals with wheatsheaf morphology were formed when the water content was further increased to H_2O/Al_2O_3 = 280 (Figures 9d and 10d: W-16). The change of morphology and increment in particle size could be explained by the dilution of nutrient when the water content increased. As a result, the low concentration of nutrients in the synthesis medium favors the crystal growth more than nucleation process. Hence, particles with larger size and different morphology are formed [35].

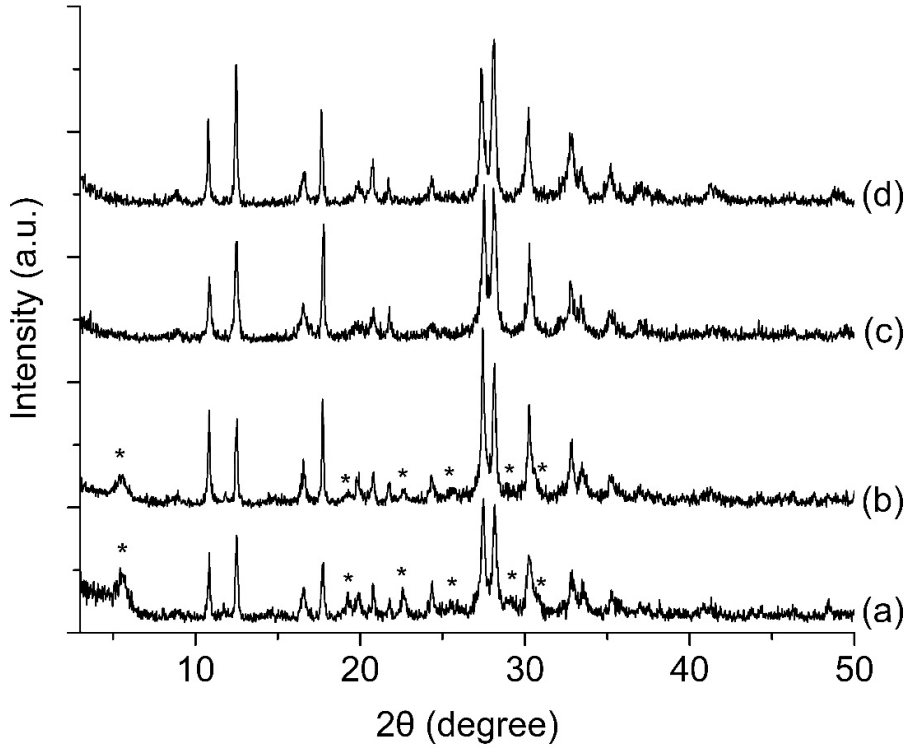

Figure 9. XRD patterns of (**a**) W-14, (**b**) W-12, (**c**) W-3 and (**d**) W-16 samples prepared from an aluminosilicate precursor hydrogel with a composition of $7SiO_2$: $1Al_2O_3$: $3.5K_2O$: zH_2O with z = 100, 130, 196 and 280, respectively. All samples were heated at 180 °C for 14 h. The * marks in (**a**,**b**) indicate the presence of the LTL crystalline phase.

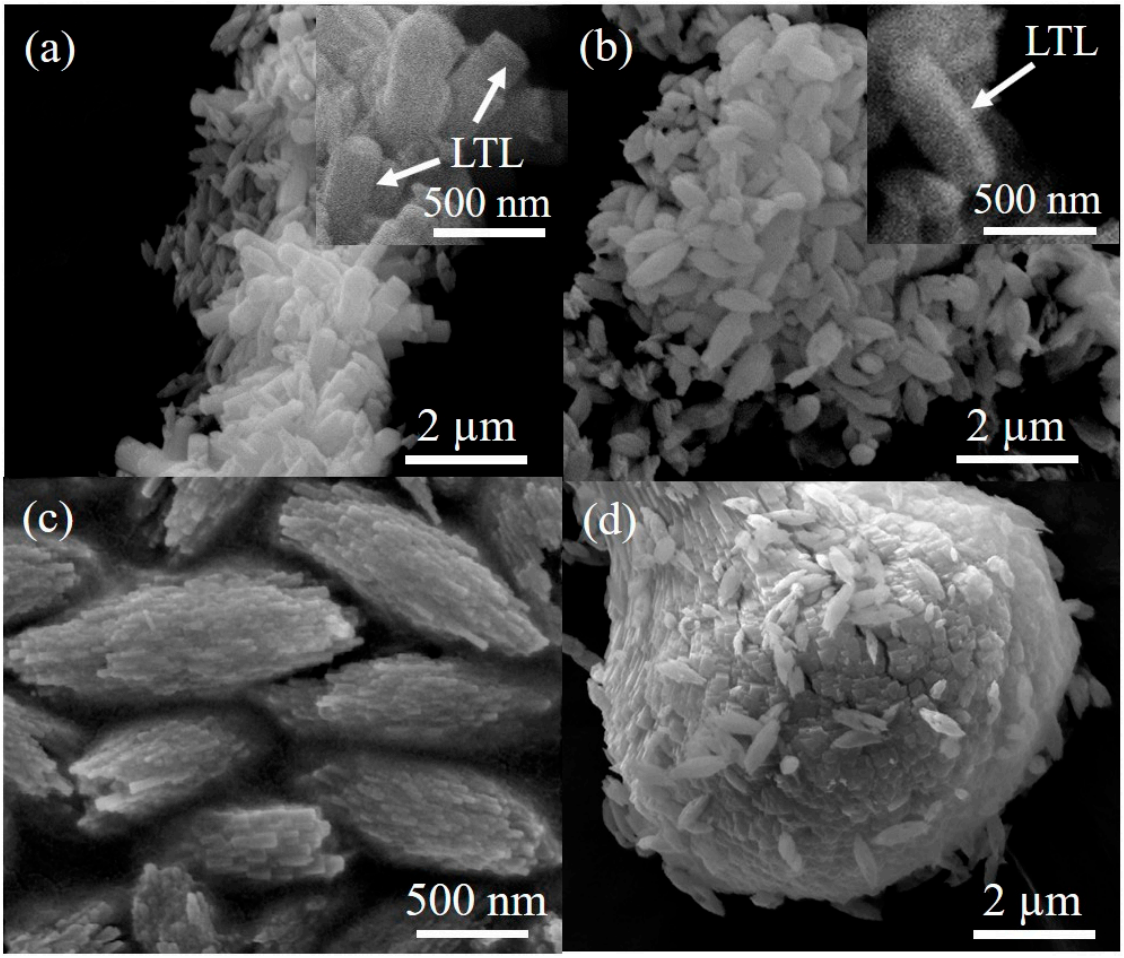

Figure 10. FESEM images of (**a**) W-14, (**b**) W-12, (**c**) W-3 and (**d**) W-16 samples solids prepared using a gel precursor of $7SiO_2$:$1Al_2O_3$:$3.5K_2O$: zH_2O at 180 °C for 14 h where z = 100, 130, 196 and 280, respectively.

3.6. Morphological Effects on the Catalytic Behavior of K-MER Zeolite

By changing the synthesis parameters, K-MER zeolites with four distinct morphologies, namely nanorod (W-3), bullet-like (W-4), prismatic (W-9) and wheatsheaf-like (W-16) shapes, were obtained. Nevertheless, from the elemental analysis, all the samples exhibited nearly similar Si/Al ratio (ca. 2.29), which was close to the theoretical one (2.12) (Table 2) [36]. Furthermore, the K/Al ratio of all the samples was found to be near unity due to the fact that the positive charge of each K^+ non-framework cation has to be counter-balanced by a negative charge contributed by an Al atom in the $[Si\text{-}O\text{-}Al]^-$ form [25]. On the other hand, the total surface area of the samples was measured with the N_2 adsorption isotherm analysis. Note that the total surface area determined was actually contributed only by the external surfaces because the size of N_2 molecules is too large to probe the micropores of the K-MER zeolite [27,37]. The results indicated that the external surface area had positive correlation with the crystallite size of K-MER zeolite. For instance, K-MER zeolite with nanorod shape had the highest external surface area (39.57 m^2/g) and the external surface area generally reduced as the crystallite size increased.

The surface basicity of these four zeolite samples was also characterized by using CO_2-TPD. Upon CO_2 adsorption and desorption from all samples, four deconvoluted signals with different intensities were observed indicating that the morphology had considerable effects on the basic strengths (weak basic sites: ca. 105 and 175 °C; medium basic sites: ca. 260 °C, medium-strong: 330 °C) (Figure 11). The number of active sites with different basic strengths was also quantified based on the amount of CO_2 sorbed per gram of zeolite (Table 2). It was found that the number of total active sites (weak,

medium and medium-strong basic strengths) was linearly proportional to the surface area of K-MER zeolite (R^2 = 0.954). In fact, this is not surprising because most of the accessible basic sites, namely $[Si\text{-}O\text{-}Al]^-K^+$, are located at the external surfaces of the zeolite particles. As a result, K-MER zeolite with smaller crystallite size exhibited a larger number of basic sites [38]. In addition, the low Si/Al ratio of the zeolite framework also contributed to the basicity of K-MER zeolite because when the Si/Al ratio is low, more K^+ cations are needed by the zeolite for surface charge counter-balance, which leads to the enhancement of zeolite basicity. Nanorod-shaped K-MER zeolite appeared to have the largest number of medium-strong basic sites (2.03 mmol/g) followed by prismatic (0.94 mmol/g), wheatsheaf-like (0.65 mmol/g) and bullet-like (0.27 mmol/g) K-MER zeolite.

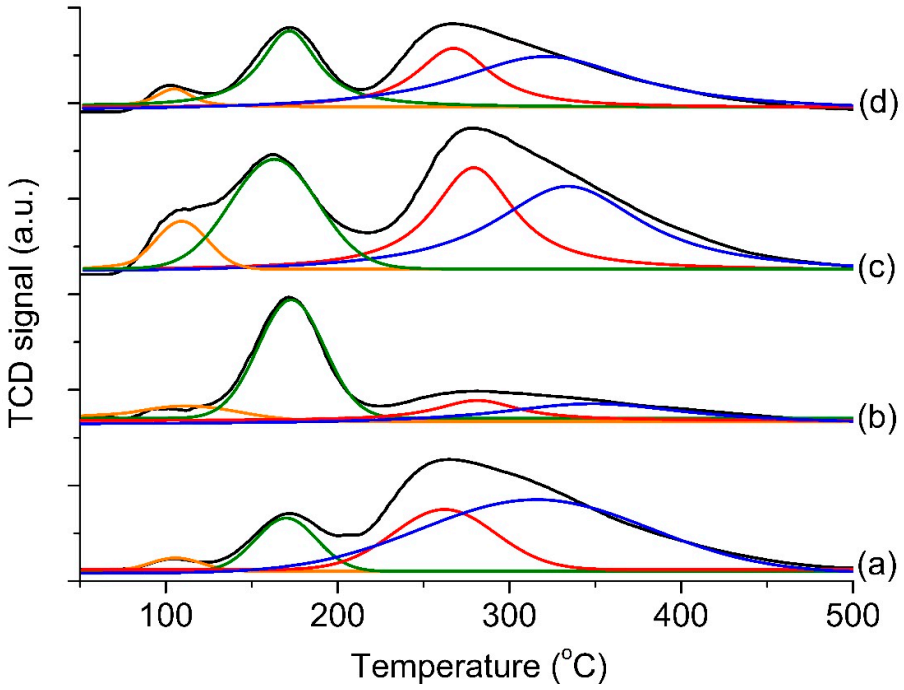

Figure 11. TPD-CO_2 profiles of (**a**) nanorod (W-3), (**b**) bullet-like (W-4), (**c**) prismatic (W-9), and (**d**) wheatsheaf-like K-MER zeolites.

Table 2. TPD-CO_2 basicity of K-MER zeolites with various morphologies.

Sample	Morphology	Si/Al Ratio	K/Al Ratio	Surface Area (m^2/g) [a]	TPD-CO_2 Basicity (mmol/g)			
					Weak	Medium	Medium-Strong	Total
W-3	Nanorod	2.29	1.04	39.57	0.08	1.99	2.03	3.10
W-4	Bullet	2.28	1.07	12.24	0.18	0.95	0.27	1.39
W-9	Prismatic	2.28	0.97	26.63	0.24	1.53	0.94	2.71
W-16	Wheatsheaf	2.31	1.06	9.01	0.04	0.56	0.65	1.25

[a] Equivalent to external surface area because micropore surface area was not measureable due to small micropore size of K-MER zeolite.

To study the morphological influences on the catalytic properties, the K-MER zeolites were tested in a model base-catalyzed reaction, i.e., cyanoethylation of methanol. The cyanoethylation of methanol with acrylonitrile was carried out under non-microwave instant heating where K-MER zeolites with different morphologies (W-3, W-4, W-9 and W-16) were used as the base catalysts (Figure 12). In general, the catalytic reactivity had a strong correlation with the morphology of zeolite catalysts. Remarkably, K-MER zeolite nanorods (W-3) exhibited superior catalytic activity with 94.1% of methanol conversion (100% selectivity) within 45 min of reaction at 140 °C, which could be explained by the largest number of accessible basic sites (particularly medium-strong basic sites) at its external surface. In contrast,

bullet-like K-MER zeolite catalyst (W-4), which had the largest crystallite size and the lowest number of basic sites, showed the lowest catalytic conversion (44.2%) among the four K-MER zeolites studied. Hence, the results showed that the morphological properties had a direct influence on the catalytic activity of a zeolite whereby the morphology is directly associated with the number of accessible catalytic active sites [39]. Comprehensive work on the aspects of molecular diffusion on K-MER zeolites with different morphologies is in progress.

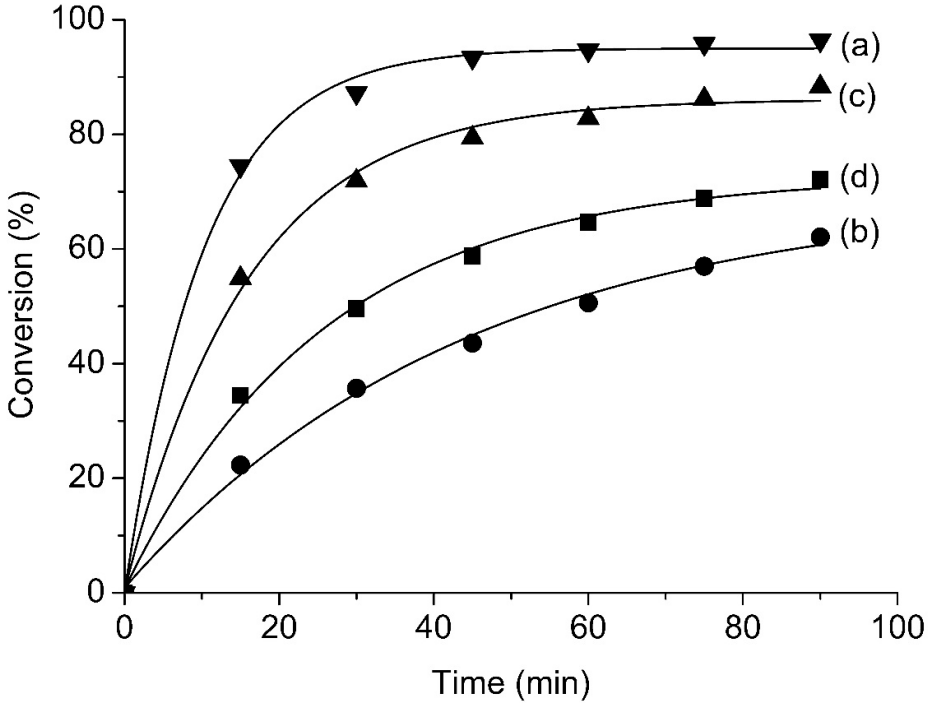

Figure 12. Catalytic performance of (**a**) nanorod (W-3), (**b**) bullet-like (W-4), (**c**) prismatic (W-9), and (**d**) wheatsheaf-like K-MER zeolites on cyanoethylation of methanol at 140 °C.

4. Conclusions

In conclusion, the effects of synthesis parameters on the crystallization profiles of K-MER zeolite have been investigated. The results reveal that the chemical composition of hydrogel (silica content, water concentration, and mineralizer loading), hydrothermal synthesis time and temperature are found to have many profound effects on the physico-chemical properties of the solid samples such as nucleation and crystallization rates, crystallite size, crystalline phase, purity and morphological properties. By carefully tuning the synthesis conditions, K-MER zeolites with four distinct morphologies, namely nanorod, bullet-like, prismatic and wheatsheaf-like shapes, have been successfully prepared. Furthermore, the influence of morphological properties of K-MER zeolites on their catalytic behavior has also been investigated. The results reveal that K-MER zeolite with nanorod shape gives the best catalytic performance in the cyanoethylation of methanol (94.1%) where its catalytic activity is associated with its stronger and higher number of accessible basic sites located at the external surface. Hence, from a material engineering point of view, this work not only provides an insight on the crystallization process of zeolite but also provides insights on designing zeolites with specific morphologies for advanced applications such as high throughput membranes for catalysis and selective gas separation.

Author Contributions: Y.-W.C.: Performed most of the experiments, wrote the manuscript; F.K., T.C.L. and E.-P.N.: wrote and proof-read the manuscript supervised; Y.-W.C.; conceived the entire project, applied for research funding; K.-L.W. and B.S.O.: ran XRD, SEM investigation, proofread the manuscript. All authors have read and agreed to the published version of the manuscript.

Funding: The financial support from a FRGS (203/PKIMIA/6711642) grant is gratefully acknowledged. Y.-W. Cheong would also like to thank the USM Fellowship for the scholarship provided.

Conflicts of Interest: The authors declare no conflict of interest.

References

1. Davis, M.E. Ordered porous materials for emerging applications. *Nature* **2002**, *417*, 813–821. [CrossRef] [PubMed]
2. Saqib, N.U.; Adnan, R.; Shah, I. Zeolite supported TiO_2 with enhanced degradation efficiency for organic dye under household compact fluorescent light. *Mater. Res. Exp.* **2019**, *6*, 095506. [CrossRef]
3. Derakhshankhah, H.; Hajipour, M.J.; Barzegari, E.; Lotfabadi, A.; Ferdousi, M.; Saboury, A.A.; Ng, E.-P.; Raoufi, M.; Awala, H.; Mintova, S.; et al. Zeolite nanoparticles inhibit Aβ–fibrinogen interaction and formation of a consequent abnormal structural clot. *ACS Appl. Mater. Interfaces* **2016**, *8*, 30768–30779. [CrossRef] [PubMed]
4. Majano, G.; Ng, E.-P.; Lakiss, L.; Mintova, S. Nanosized molecular sieves utilized as an environmentally friendly alternative to antioxidants for lubricant oils. *Green Chem.* **2011**, *13*, 2435–2440. [CrossRef]
5. Balkus, K.J., Jr.; Shi, J. A study of suspending agents for gadolinium (III)-exchanged hectorite. An oral magnetic resonance imaging contrast agent. *Langmuir* **1996**, *12*, 6277–6281. [CrossRef]
6. Adam, F.; Appaturi, J.N.; Ng, E.-P. Halide aided synergistic ring opening mechanism of epoxides and their cycloaddition to CO_2 using MCM-41-imidazolium bromide catalyst. *J. Mol. Catal. A Chem.* **2014**, *386*, 42–48. [CrossRef]
7. Ng, E.-P.; Lim, G.K.; Khoo, G.-L.; Tan, K.-H.; Ooi, B.S.; Adam, F.; Ling, T.C.; Wong, K.-L. Synthesis of colloidal stable Linde Type J (LTJ) zeolite nanocrystals from rice husk silica and their catalytic performance in Knoevenagel reaction. *Mater. Chem. Phys.* **2015**, *155*, 30–35. [CrossRef]
8. Ng, E.-P.; Nur, H.; Wong, K.-L.; Muhid, M.N.M.; Hamdan, H. Generation of Brönsted acidity in AlMCM-41 by sulphation for enhanced liquid phase tert-butylation of phenol. *Appl. Catal. A Gen.* **2007**, *323*, 58–65. [CrossRef]
9. Kakutani, Y.; Weerachawanasak, P.; Hirata, Y.; Sano, M.; Suzuki, T.; Miyake, T. Highly effective K-Merlinoite adsorbent for removal of Cs^+ and Sr^{2+} in aqueous solution. *RSC Adv.* **2017**, *7*, 30919–30928. [CrossRef]
10. Mirfendereski, S.M. Synthesis and application of high-permeable MER zeolite membrane for separation of carbon dioxide from methane. *J. Aust. Ceram. Soc.* **2019**, *55*, 103–114. [CrossRef]
11. Seo, Y.H.; Prasetyanto, E.A.; Jiang, N.; Oh, S.M.; Park, S.E. Catalytic dehydration of methanol over synthetic K-MER zeolite. *Microporous Mesoporous Mater.* **2010**, *128*, 108–114. [CrossRef]
12. Cheong, Y.-W.; Wong, K.-L.; Ling, T.C.; Ng, E.-P. Rapid synthesis of nanocrystalline zeolite W with hierarchical mesoporosity as an efficient solid basic catalyst for nitroaldol Henry reaction of vanillin with nitroethane. *Mater. Express* **2018**, *8*, 463–468. [CrossRef]
13. Liu, X.-D.; Wang, Y.-P.; Cui, X.-M.; He, Y.; Mao, J. Influence of synthesis parameters on NaA zeolite crystals. *Powder Technol.* **2013**, *243*, 184–193. [CrossRef]
14. Sivalingam, S.; Sen, S. Optimization of synthesis parameters and characterization of coal fly ash derived microporous zeolite X. *Appl. Surf. Sci.* **2018**, *455*, 903–910. [CrossRef]
15. Quan, Y.; Li, S.; Wang, S.; Li, Z.; Dong, M.; Qin, Z.; Chen, G.; Wei, Z.; Fan, W.; Wang, J. Synthesis of chainlike ZSM-5 zeolites: Determination of synthesis parameters, mechanism of chainlike morphology formation, and their performance in selective adsorption of xylene isomers. *ACS Appl. Mater. Interfaces* **2017**, *9*, 14899–14910. [CrossRef]
16. Au, L.T.Y.; Yeung, K.L. An investigation of the relationship between microstructure and permeation properties of ZSM-5 membranes. *J. Membr. Sci.* **2001**, *194*, 33–55. [CrossRef]
17. Li, S.; Li, J.; Dong, M.; Fan, S.; Zhao, T.; Wang, J.; Fan, W. Strategies to control zeolite particle morphology. *Chem. Soc. Rev.* **2019**, *48*, 885–907. [CrossRef]

18. Jhung, S.H.; Chang, J.-S.; Hwang, Y.K.; Park, S.-E. Crystal morphology control of AFI type molecular sieves with microwave irradiation. *J. Mater. Chem.* **2004**, *14*, 280–285. [CrossRef]
19. Khoo, D.Y.; Kok, W.-M.; Mukti, R.R.; Mintova, S.; Ng, E.-P. Ionothermal approach for synthesizing AlPO-5 with hexagonal thin-plate morphology influenced by various parameters at ambient pressure. *Solid State Sci.* **2013**, *25*, 63–69. [CrossRef]
20. Ng, E.-P.; Ng, D.T.-L.; Awala, H.; Wong, K.-L.; Mintova, S. Microwave synthesis of colloidal stable AlPO-5 nanocrystals with high water adsorption capacity and unique morphology. *Mater. Lett.* **2014**, *132*, 126–129. [CrossRef]
21. Ou, X.; Xu, S.; Warnett, J.M.; Holmes, S.M.; Zaheer, A.; Garforth, A.A.; Williams, M.A.; Jiao, Y.; Fan, X. Creating hierarchies promptly: Microwave-accelerated synthesis of ZSM-5 zeolites on macrocellular silicon carbide (SiC) foams. *Chem. Eng. J.* **2017**, *312*, 1–9. [CrossRef]
22. Askari, S.; Halladj, R. Ultrasonic pretreatment for hydrothermal synthesis of SAPO-34 nanocrystals. *Ultrason. Sonochem.* **2012**, *19*, 554–559. [CrossRef] [PubMed]
23. Ng, E.-P.; Chow, J.-H.; Mukti, R.R.; Muraza, O.; Ling, T.C.; Wong, K.-L. Hydrothermal synthesis of zeolite a from bamboo leaf biomass and its catalytic activity in cyanoethylation of methanol under autogenic pressure and air conditions. *Mater. Chem. Phys.* **2017**, *201*, 78–85. [CrossRef]
24. Ginés-Molina, M.J.; Ahmad, N.H.; Mérida-Morales, S.; García-Sancho, C.; Mintova, S.; Ng, E.-P.; Maireles-Torres, P. Selective Conversion of Glucose to 5-Hydroxymethylfurfural by Using L-Type Zeolites with Different Morphologies. *Catalysts* **2019**, *9*, 1073. [CrossRef]
25. Ghrear, T.M.A.; Rigolet, S.; Daou, T.J.; Mintova, S.; Ling, T.C.; Tan, S.H.; Ng, E.-P. Synthesis of Cs-ABW nanozeolite in organotemplate-free system. *Microporous Mesoporous Mater.* **2019**, *277*, 78–83. [CrossRef]
26. Wong, S.-F.; Awala, H.; Vincente, A.; Retoux, R.; Ling, T.C.; Mintova, S.; Mukti, R.R.; Ng, E.-P. KF zeolite nanocrystals synthesized from organic-template-free precursor mixture. *Microporous Mesoporous Mater.* **2017**, *249*, 105–110. [CrossRef]
27. IZA-SC Database of Zeolite Structures. Available online: http://www.iza-structure.org/databases/ (accessed on 1 December 2019).
28. Wong, S.-F.; Deekomwong, K.; Wittayakun, J.; Ling, T.C.; Muraza, O.; Adam, F.; Ng, E.-P. Crystal growth study of KF nanozeolite and its catalytic behavior in Aldol condensation of benzaldehyde and heptanal enhanced by microwave heating. *Mater. Chem. Phys.* **2017**, *196*, 295–301. [CrossRef]
29. Ng, E.-P.; Sekhon, S.S.; Mintova, S. Discrete MnAlPO-5 nanocrystals synthesized by an ionothermal approach. *Chem. Commun.* **2009**, 1661–1663. [CrossRef]
30. Ng, E.-P.; Awala, H.; Ghoy, J.P.; Vicente, A.; Ling, T.C.; Ng, Y.H.; Mintova, S.; Adam, F. Effects of ultrasonic irradiation on crystallization and structural properties of EMT-type zeolite nanocrystals. *Mater. Chem. Phys.* **2015**, *159*, 38–45. [CrossRef]
31. Zhang, J.; Lu, X.; Wang, Z. Control of crystallization rate and morphology of zeolite silicalite-1 in solvent-free synthesis. *Microporous Mesoporous Mater.* **2019**, *283*, 14–24. [CrossRef]
32. Ng, E.-P.; Rigolet, S.; Daou, T.J.; Mintova, S.; Ling, T.C. Micro-and macroscopic observations of the nucleation process and crystal growth of nanosized Cs-pollucite in an organotemplate-free hydrosol. *New J. Chem.* **2019**, *43*, 17433–17440. [CrossRef]
33. Gomez, A.G.; de Silveira, G.; Doana, H.; Cheng, C.-H. A facile method to tune zeolite L crystals with low aspect ratio. *Chem. Commun.* **2011**, *47*, 5876–5878. [CrossRef] [PubMed]
34. Ng, E.-P.; Goh, J.-Y.; Ling, T.C.; Mukti, R.R. Eco-friendly synthesis for MCM-41 nanoporous materials using the non-reacted reagents in mother liquor. *Nanoscale Res. Lett.* **2013**, *8*, 120. [CrossRef] [PubMed]
35. Ghrear, T.M.A.; Cheong, Y.-W.; Lim, G.K.; Chateigner, D.; Ling, T.C.; Tan, S.H.; Ng, E.-P. Fast, low-pressure, low-temperature microwave synthesis of ABW cesium aluminosilicate zeolite nanocatalyst in organotemplate-free hydrogel system. *Mater. Res. Bull.* **2020**, *122*, 110691. [CrossRef]
36. Barrett, P.A.; Valencia, S.; Camblor, M.A. Synthesis of a merlinoite-type zeolite with an enhanced Si/Al ratioviapore filling with tetraethylammonium cations. *J. Mater. Chem.* **1998**, *8*, 2263–2268. [CrossRef]
37. Mohammad, S.A.G.; Khoerunnisa, F.; Rigolet, S.; Daou, T.J.; Ling, T.C.; Ng, E.-P. Hierarchical Cs–Pollucite Nanozeolite Modified with Novel Organosilane as an Excellent Solid Base Catalyst for Claisen–Schmidt Condensation of Benzaldehyde and Acetophenone. *Processes* **2020**, *8*, 96. [CrossRef]

38. Choo, M.-Y.; Juan, J.C.; Oi, L.E.; Ling, T.C.; Ng, E.-P.; Noorsaadah, A.R.; Centi, G.; Lee, K.T. The role of nanosized zeolite Y in the H 2-free catalytic deoxygenation of triolein. *Catal. Sci. Technol.* **2019**, *9*, 772–782. [CrossRef]
39. Hargreaves, J.S.J.; Hutchings, G.J.; Joyner, R.W.; Kiely, C.J. The relationship between catalyst morphology and performance in the oxidative coupling of methane. *J. Catal.* **1992**, *135*, 576–595. [CrossRef]